

Adaptive Time-Domain Harmonic Control for Noise-Vibration-Harshness Reduction of Electric Drives

Klaus Herburger¹, Fabian Jakob², David Gänzle¹, Maximilian Manderla¹, Andrea Iannelli²

Abstract—Reducing Noise, Vibration, and Harshness (NVH) in electric drives is crucial for applications such as electric vehicle drivetrains and heat-pump compressors, where strict NVH requirements directly affect user satisfaction and component longevity. This work presents the integration of an adaptive time-domain harmonic controller into an existing electric-drive control loop to attenuate harmonic disturbances. Three control structures are proposed and analyzed, along with a modified parameter-estimation scheme that reduces computational effort while preserving estimation accuracy, making the method suitable for embedded real-time implementation. To cope with fast operating-point changes, a delta-learning approach combines adaptive control with a lookup-table-based feedforward estimator, ensuring fast convergence and robustness. The proposed controller architectures are validated through simulation and testbench experiments on a permanent-magnet synchronous machine drive, demonstrating substantial NVH reductions across operating conditions. The results confirm that time-domain adaptive harmonic control offers a practical and theoretically grounded solution for real-time NVH mitigation in electric drives.

I. INTRODUCTION

Addressing Noise, Vibration, and Harshness (NVH) in electric drives is crucial for the electrification of mobility and heating. Beyond user comfort, mitigating NVH also extends component lifetime. At low speeds, electromagnetic NVH dominates, which is caused by harmonic oscillations in forces and inverter voltages at multiples of the rotor's electrical frequency [1]–[3].

NVH mitigation can be achieved either through constructive design or control-based methods [4]. Inspired by harmonic disturbance rejection algorithms from other domains [5]–[8], this work investigates a control-based approach: injecting sinusoidal control inputs at disturbance frequencies to cancel their effect. Implementation is challenged by the unknown current-to-NVH transfer behavior and unmeasurable disturbances. However, surface accelerations, measurable e.g. by MEMS sensors, can be used as surrogate signals to quantify the NVH. They can therefore be utilized for offline or online estimation of the unknown transfer behavior.

An adaptive control approach is appealing in this context due to its ability to estimate system dynamics online.

¹ Corporate Research, Robert Bosch GmbH, 71272 Renningen, Germany. klaus.herburger@de.bosch.com; david.gaenzle@de.bosch.com; maximilian.manderla@de.bosch.com

² University of Stuttgart, Institute for Systems Theory and Automatic Control, 70550 Stuttgart, Germany. fabian.jakob@ist.uni-stuttgart.de; andrea.iannelli@ist.uni-stuttgart.de

Corresponding author: Klaus Herburger (klaus.herburger@de.bosch.com)

It maintains performance despite aging or temperature drift and reduces calibration effort, addressing key challenges in electric drives. However, integrating adaptive controllers into electric drive control is non-trivial: the additional controller must coexist with existing ones without interference, be computationally efficient for embedded real-time execution, and converge rapidly to cope with changes in transfer behavior across operating points. This work addresses these challenges in the context of Permanent-Magnet Synchronous Machine (PSM) drives.

A. Related work

Many methods for harmonic disturbance rejection in unknown systems have been proposed. If the open-loop dynamics between control input and measurement signal is asymptotically stable and partial model knowledge is available, adaptive feedforward cancellation can be applied [9]. Feedback-based adaptive approaches are also possible but typically rely on model assumptions such as known relative degree or minimum-phase behavior [10].

A widely used alternative is Harmonic Control (HC), developed independently across several research fields, which neglects transients and reduces the problem to disturbance attenuation in the Harmonic Steady State (HSS) [11]–[14]. Classical HC requires sufficiently accurate phase knowledge of the transfer function to ensure stability, which is often difficult to obtain. To address this, adaptive HC methods have been proposed [15]. In frequency-domain adaptive HC, amplitudes and phases are extracted using a Discrete Fourier Transformation (DFT) [16]. While effective, the large update period required for stability leads to slow convergence [6], [15].

Time-domain adaptive HC avoids this limitation by working directly with the measured signal. The stability was initially shown using averaging arguments [17]; but also a more sophisticated Lyapunov-proof has arisen [18], which was used to demonstrate that larger adaptation gains can be used compared to frequency-domain adaptive HC.

Building on these results, this work employs time-domain adaptive HC, as it achieves stability without model knowledge and offers faster convergence than frequency-domain methods.

B. Objective and contribution

This work investigates the integration of time-domain adaptive HC into the control loop of an electric drive, with

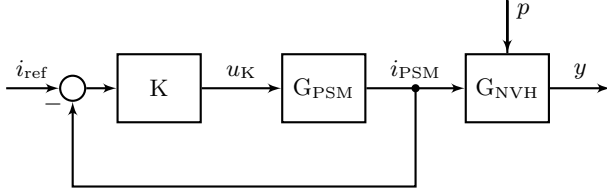


Fig. 1. Control loop without HC.

emphasis on a theoretically sound design that guarantees stability of both the adaptive controller and the overall system. The approach is validated through simulations and testbench experiments.

To overcome the key challenges of controller coexistence, computational efficiency, and robustness under varying operating points, the main contributions are:

- **Controller coexistence:** Development of three control structures that integrate adaptive time-domain HC for NVH reduction while ensuring compatibility with the existing control loop.
- **Computational efficiency:** Modification of the estimation scheme to reduce matrix multiplications, achieving equal estimation accuracy with improved suitability for embedded real-time implementation.
- **Robustness to operating changes:** Introduction of a delta learning approach that combines adaptive time-domain HC with a Lookup Table (LUT)-based feedforward estimator. An adaptive LUT enables online updates that reflect parameter changes due to aging.
- **Experimental validation:** Implementation and testing of the proposed control structures on an e-drive testbench, confirming their feasibility and effectiveness under real operating conditions.

C. Outline

Section II introduces preliminaries, before Section III presents the integration of the adaptive time-domain HC and its parameter estimator, followed by a stability analysis. Section IV introduces the delta learning approach. The concepts are validated through simulations (Section V) and testbench experiments (Section VI), before conclusions are drawn in Section VII.

II. PRELIMINARIES

The typical control loop of a PSM is illustrated in Figure 1. Here i_{ref} is a current that is typically pre-generated to match some reference torque T_{ref} . The controller K regulates the currents by adjusting the voltages supplied to the PSM, represented by the plant model G_{PSM} [19]. The NVH emissions of the electric drive are represented by surface vibration quantities, denoted by y . They are modelled by an unknown, asymptotically stable Linear Time Invariant (LTI) transfer function G_{NVH} characterizing the dynamic behavior of the NVH signal with input i_{PSM} and an additive external unmeasured output disturbance p as

$$y = G_{\text{NVH}} i_{\text{PSM}} + p. \quad (1)$$

Note that i_{PSM} is only indirectly controllable.

A. Harmonic oscillations and NVH in electric drives

Since G_{NVH} is asymptotically stable, the transient response y_{trans} of the measured NVH emissions vanishes. Thus, the total response y approaches its harmonic steady-state component y_{hss} asymptotically [20], which is defined as

$$y_{\text{hss}}(t) = \sum_{i=1}^q f_i^T(t) \theta_{y,i}, \quad (2)$$

$$f_i(t) = \begin{bmatrix} \sin(\omega_i t) \\ \cos(\omega_i t) \end{bmatrix}, \quad \theta_{y,i} = \begin{bmatrix} \theta_{y,s,i} \\ \theta_{y,c,i} \end{bmatrix} \in \mathbb{R}^2.$$

The goal is to achieve $y_{\text{hss}}(t) = 0$. In (2), $\omega_i > 0$ are the disturbance frequencies, which must be known to apply harmonic control. NVH in electric machines are typically caused by harmonic oscillations in the electromagnetic forces and inverter voltages [2] [3]. Crucially, empirical findings show that those oscillations occur at frequencies $\omega_{\text{el},m} = m\omega_{\text{el}}$ that are multiple integers of the known electrical frequency ω_{el} [2] [3]. The problem of mitigating harmonics at different frequencies can be considered decoupled from each other, therefore we refer to any $\omega_{\text{el},m}$ as just ω_i in the following. Moreover, considering currents in the dq-coordinate system, it has been observed that NVH is primarily induced by the q -component i_q [21]. Thus, for the remainder of this work, we consider one-dimensional control inputs. Extensions to multidimensional signals exist and are straightforward, which may be explored when two independent measurements y_1 and y_2 are available and if both the d and q component shall be exploited [18].

B. Harmonic control

In HC it is assumed to have access to a control input u and a measureable performance signal y for which a dynamic relation

$$y(t) = G_{u \rightarrow y}(s)[u(t)] + p(t), \quad (3)$$

with unknown disturbance p holds. Crucially, all signals are assumed to only consist of their HSS response, i.e., the transient is neglected and

$$p(t) = \sum_{i=1}^q f_i^T(t) \theta_{p,i} \quad u(t) = \sum_{i=1}^q f_i(t)^T \theta_{u,i}. \quad (4)$$

Using linear system theory [20], it can be shown that the HSS response of (3) results in

$$y(t) = \sum_{i=1}^q f_i^T(t) (G_i \theta_{u,i} + \theta_{p,i}) \quad (5)$$

with

$$G_i = \begin{bmatrix} \text{Re } G_{u \rightarrow y}(j\omega_i) & -\text{Im } G_{u \rightarrow y}(j\omega_i) \\ \text{Im } G_{u \rightarrow y}(j\omega_i) & \text{Re } G_{u \rightarrow y}(j\omega_i) \end{bmatrix} \in \mathbb{R}^{2 \times 2}. \quad (6)$$

The goal is to suppress harmonic steady state oscillations, and if G_i and $\theta_{p,i}$ are known, $\theta_{u,i}$ can be calculated as

$$\theta_{u,i} = -G_i^{-1} \theta_{p,i} \quad (7)$$

to achieve $y_{\text{hss}} = 0$, making the approach both intuitive and straightforward. In our setup however, the main challenge is to estimate the unknown transfer function G_i and the unknown disturbance $\theta_{p,i}$ at the relevant frequencies. Since G_i and $\theta_{p,i}$ change online due to varying operating points and aging effects, it is desirable to estimate them in real-time, yielding an adaptive control scheme. Note that adaptive HC approaches have already been studied — see, e.g., [16]–[18], where the transfer matrix G_i is estimated online. Building on these preliminaries, the following section discusses how the adaptive time-domain HC can be integrated into the control loop of the electric drive.

III. ADAPTIVE TIME-DOMAIN HC IN ELECTRIC DRIVES: CONTROL STRUCTURES, ESTIMATION, AND STABILITY

This section develops the core contribution of this work: the integration of adaptive time-domain HC into the control structure of electric drives to reduce NVH emissions.

A. Integration into the control loop

The objective is to incorporate an adaptive time-domain HC into the control loop to mitigate NVH emissions without affecting the existing controller K . The input to the unknown system i_{PSM} cannot be manipulated directly, but only through the control voltages u_K . Three control structures are proposed, where each structure offers unique advantages/disadvantages and may be favored based on the application and on which parts of the control loop may be accessible. In all control structures, the system formulation (3) is used, but u and $G_{u \rightarrow y}$ vary depending on the structure.

1) *Structure 1 – Acceleration to voltage*: In Structure 1 the control output is the voltage u_{HC} that is added to u_K to get u_{PSM} , as illustrated in Figure 2a. The unknown system results in

$$y = G_{u_{\text{PSM}} \rightarrow y} u_{\text{PSM}} + p, \quad (8)$$

i.e., $u = u_{\text{PSM}}$ and $G_{u \rightarrow y} = G_{u_{\text{PSM}} \rightarrow y} = G_{i_{\text{PSM}} \rightarrow y} G_{\text{PSM}}$. This approach has the advantage that frequency-domain HC concepts as in [16] can be implemented with the same control structure. The disadvantage is that the known model G_{PSM} is not leveraged in the HC, since it treats this part of the system as unknown. Crucially, a decoupling block \hat{G}_{PSM} avoids that K and HC influence each other due to their conflicting control goals. Specifically,

$$i_{\text{HC}} = \hat{G}_{\text{PSM}} u_{\text{HC}} \quad (9)$$

ensures that the transfer behavior from i_{ref} to i_{PSM} remains the closed loop transfer behavior of the nominal control structure. If \hat{G}_{PSM} is equal to G_{PSM} , then

$$\begin{aligned} i_K &= i_{\text{ref}} - i_{\text{PSM}} + i_{\text{HC}} \\ &= i_{\text{ref}} - G_{\text{PSM}}(u_K + u_{\text{HC}}) + \hat{G}_{\text{PSM}} u_{\text{HC}} \\ &= (1 + G_{\text{PSM}} K)^{-1} i_{\text{ref}}, \end{aligned} \quad (10)$$

which corresponds exactly to the nominal control structure. Accurate models are reasonable assumptions in e-drives, however, care must be taken for model mismatches regarding the feedforward prediction.

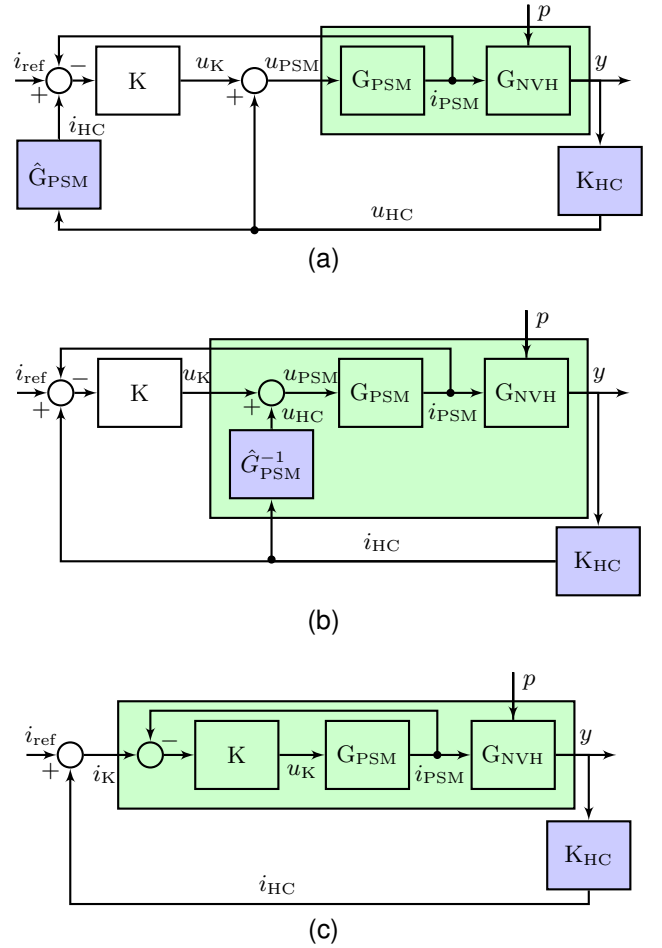


Fig. 2. Control architectures considered in this work. The shaded area indicates the part of the system assumed unknown. (a) Structure 1 – Acceleration to voltage. (b) Structure 2 – Acceleration to measured current. (c) Structure 3 – Acceleration to reference current.

2) *Structure 2 – Acceleration to measured current*: Structure 2 aims at estimating the transfer behavior from i_{PSM} to y . Thus, the output of the controller is the current that would need to be added to i_{PSM} . Since it is not possible to control i_{PSM} directly, the control output i_{HC} is converted to u_{HC} using an inverse model of the PSM that is denoted as $\hat{G}_{\text{PSM}}^{-1}$. The control loop for Structure 2 is shown in Figure 2b. It considers

$$\begin{aligned} y &= G_{i_{\text{HC}} \rightarrow y} i_{\text{HC}} + p \\ &= G_{i_{\text{PSM}} \rightarrow y} G_{\text{PSM}} \hat{G}_{\text{PSM}}^{-1} i_{\text{HC}} + p \end{aligned} \quad (11)$$

as the unknown system that is to be estimated. To implement $\hat{G}_{\text{PSM}}^{-1}$, a time delay is introduced at the input to avoid acausality in the inverse PSM model. If the condition $G_{\text{PSM}} \hat{G}_{\text{PSM}}^{-1} = 1$ holds, the HC does not influence K , if i_{HC} is subtracted from i_{PSM} . Then, only the current resulting from u_K remains in the feedback loop of K and (10) holds. The main advantage of Structure 2 over Structure 1 is then that the PSM is not part of the estimated system.

3) *Structure 3 – Acceleration to reference current*: Another way to achieve that the PSM is not part of the estimated system is to add the control output i_{HC} to the reference current i_{ref} to get i_K . Structure 3 does – in contrast to the other two structures – not need an exact model of G_{PSM} to achieve the decoupling

TABLE I
OVERVIEW OF THE THREE CONTROL STRUCTURES.

Method	Input	Main advantage	Main disadvantage
Structure 1	u_{PSM}	Similar to frequency-domain structure	PSM model is assumed unknown
Structure 2	i_{PSM}	System assumed unknown equals the unknown system	PSM model needs to be known exactly for full decoupling
Structure 3	i_K	No controller decoupling necessary	K closed loop is assumed unknown

of the controllers. The resulting control structure is shown in Figure 2c. This results in the following representation of the unknown and to be estimated system:

$$y = G_{i_K \rightarrow y} i_K + p. \quad (12)$$

Since

$$i_{\text{PSM}} = \frac{G_{\text{PSM}} K}{1 + G_{\text{PSM}} K} i_K, \quad (13)$$

the (known) closed loop of K is part of the estimated system with

$$y = G_{i_{\text{PSM}} \rightarrow y} \frac{G_{\text{PSM}} K}{1 + G_{\text{PSM}} K} i_K + p, \quad (14)$$

which is a disadvantage of this structure.

4) *Comparison of the three control structures:* In this section, three control structures are presented, that are designed to integrate adaptive time-domain HC techniques into the existing control loop. An overview is shown in Table I. It highlights the input u to the estimated system, the main advantage and the main disadvantage of each structure.

B. Online parameter estimation

Since the true parameters G_i^* and $\theta_{p,i}^*$ are unknown, the controller relies on their estimates G_i and $\theta_{p,i}$. An estimation scheme is proposed for the general formulation (5), thus applicable to all three control structures, and with the goal of identifying G_i and $\theta_{p,i}$ online. Define the sampled data as

$$y_k = y(kt_s), \quad f_{i,k} = f_i(kt_s) \quad (15)$$

for each $k \in \mathbb{N}$ with the sampling time t_s . Using the approximation

$$y(kt_s) = y_{\text{hss}}(kt_s, \theta_{u,1,k}, \dots, \theta_{u,q,k}), \quad (16)$$

y_k can be expressed as

$$y_k = \sum_{i=1}^q f_{i,k}^T (G_i^* \theta_{u,i,k} + \theta_{p,i}^*). \quad (17)$$

Analogously, the estimation \hat{y}_k is defined as

$$\hat{y}_k = \sum_{i=1}^q f_{i,k}^T (G_{i,k} \theta_{u,i,k} + \theta_{p,i,k}). \quad (18)$$

More compactly, we write (18) as

$$\hat{y}_k = \sum_{i=1}^q w_{i,k}^T x_{i,k}, \quad (19)$$

with the unknown parameter vector

$$x_{i,k}^T := [\text{Re } G_{u \rightarrow y}(j\omega_i)_k \quad \text{Im } G_{u \rightarrow y}(j\omega_i)_k \quad \theta_{p,s,i,k} \quad \theta_{p,c,i,k}] \quad (20)$$

and the regressor

$$w_{i,k} := \begin{bmatrix} \theta_{u,s,i,k} \sin(\omega_i k t_s) + \theta_{u,c,i,k} \cos(\omega_i k t_s) \\ \theta_{u,s,i,k} \cos(\omega_i k t_s) - \theta_{u,c,i,k} \sin(\omega_i k t_s) \\ \sin(\omega_i k t_s) \\ \cos(\omega_i k t_s) \end{bmatrix}. \quad (21)$$

Here, the subscripts “s” and “c” denote the sine and cosine components of the corresponding parameters θ_u and θ_p , respectively, as introduced in (2). We define the cost function

$$J_k(x_k) = \frac{\eta_k \|y_k - \sum_{i=1}^q w_{i,k}^T x_{i,k}\|^2}{2} = \frac{\|\epsilon_k\|^2}{2\eta_k} \quad (22)$$

which is to be minimized, where the normalization error is defined as

$$\epsilon_k = \eta_k (y_k - \hat{y}_k). \quad (23)$$

Since this a positive semi-definite quadratic cost function, standard methods with provable convergence rates can be employed. Considering the computational budget, the gradient method is used. Following [22], this leads to the adaptive law

$$x_{i,k+1} = x_{i,k} + \Gamma w_{i,k} \epsilon_k. \quad (24)$$

Here specifically, the normalization factor is chosen as

$$\eta_k = \frac{1}{1 + \sum_{i=1}^q \|\theta_{u,i,k}\|^2}. \quad (25)$$

This particular choice of the normalization factor is needed for the stability theorem in the next section and is one modification over [17]. The learning rate Γ is chosen as

$$\Gamma = \text{diag}(\gamma_G, \gamma_G, \gamma_p, \gamma_p) \quad (26)$$

to provide individual learning rates $\gamma_G, \gamma_p > 0$ for the transfer function and the disturbance parameters. Note that unlike in [18], $G_{i,k}$ and $\theta_{p,i,k}$ are estimated jointly, which will be especially beneficial in the context of computational limitations. Finally, the estimated parameters $x_{i,k}$ are then used to construct $G_{i,k}$ and $\theta_{p,i,k}$. This approach ensures that the block structure of $G_{i,k}$ is preserved without adding additional terms to the estimation equations as in [18]. In summary, the control law is given by (24) with

$$\theta_{u,i,k} = -G_{i,k}^{-1} \theta_{p,i,k}. \quad (27)$$

The control architecture is shown in Figure 3.

C. Stability theorem

Since the control law (27) is used for all $k \in \mathbb{N}$, it is also used when the parameters are incorrectly initialized. A stability theorem ensures that stability of the controller and convergence of y_k to zero can be guaranteed for all initial conditions $G_{i,0}$ and $\theta_{p,i,0}$, i.e. the same properties as in [18] can be shown for the computationally efficient estimation scheme proposed in the previous subsection.

We make the following assumptions:

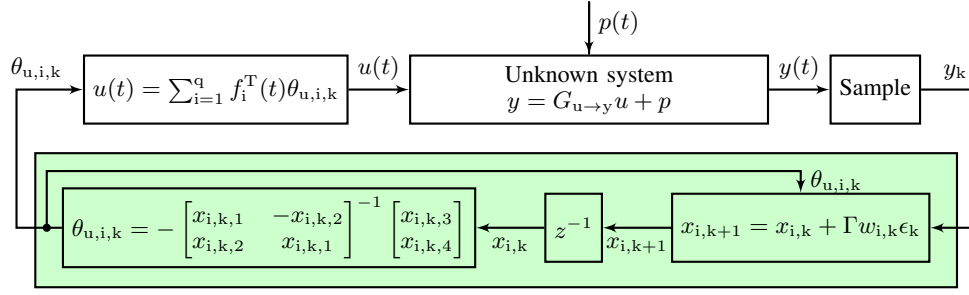


Fig. 3. Feedback interconnection with adaptive time-domain harmonic controller (inside shaded area).

Assumption 1. The following conditions hold for all $i = 1, \dots, q$ and all $k \in \mathbb{N}$:

- (1a) The transfer function satisfies $\text{rank } G_{u \rightarrow y}(j\omega_i) = l$.
- (1b) The disturbance frequencies $\omega_1, \dots, \omega_q$ are known.
- (1c) The output satisfies $y_k = y_{\text{hss}}(kt_s, \theta_{u,1,k}, \dots, \theta_{u,q,k})$.
- (1d) There exists $\epsilon > 0$ such that $\lambda_{\min}(G_{i,k} G_{i,k}^T) > \epsilon$.

Assumption (1a) implies that the number of actuators must be at least as large as the number of performance measurements. This is always fulfilled in the considered setup, since $y \in \mathbb{R}$ and $u \in \mathbb{R}$. Assumption (1b) is fulfilled, since the harmonic disturbance frequencies are known to be integer multiples of the known electrical frequency ω_{el} . The HSS assumption (1c) indicates the stability theorem is valid assuming the transient response y_{trans} vanished. Given that G_{NVH} is asymptotically stable with relatively fast dynamics, this assumption is considered to be met. Assumption (1d) infers that there exists a singularity at $(x_{i,k,1}, x_{i,k,2}) = 0$ that is to be avoided. Using

$$G_{i,k} = \begin{bmatrix} x_{i,k,1} & -x_{i,k,2} \\ x_{i,k,2} & x_{i,k,1} \end{bmatrix} \in \mathbb{R}^{2 \times 2} \quad (28)$$

with $x_{i,k,1} = \text{Re } G_{u \rightarrow y}(j\omega_i)_k$ and $x_{i,k,2} = \text{Im } G_{u \rightarrow y}(j\omega_i)_k$, it follows

$$G_{i,k} G_{i,k}^T = \begin{bmatrix} x_{i,k,1}^2 + x_{i,k,2}^2 & 0 \\ 0 & x_{i,k,1}^2 + x_{i,k,2}^2 \end{bmatrix} \quad (29)$$

and therefore

$$\lambda_{\min}(G_{i,k} G_{i,k}^T) = x_{i,k,1}^2 + x_{i,k,2}^2. \quad (30)$$

This implies $\lambda_{\min}(G_{i,k} G_{i,k}^T) > \epsilon$ if $(x_{i,k,1}, x_{i,k,2}) \neq 0$. This requirement is inherently met in the initial estimation phase if the initial values $x_{i,0,1}, x_{i,0,2}$ are chosen sufficiently large. After the initial phase the singularity can be avoided by suitable algorithm modifications, such as the addition of an arbitrary perturbation to the parameters in regions of small amplitudes or the interruption of the $x_{i,k,1}, x_{i,k,2}$ update until the gradient forces an amplitude growth again.

For the stability theorem, define the closed-loop system

$$y_k = \sum_{i=1}^q f_{i,k}^T \left(\theta_{p,i}^* - G_i^* G_{i,k}^{-1} \theta_{p,i,k} \right), \quad (31)$$

which follows when the control law (27) is plugged into the system formulation (17). Define the parameter estimation error as

$$\tilde{x}_{i,k} = x_{i,k} - \alpha x_i^*. \quad (32)$$

The following theorem provides the stability conditions for the closed-loop system.

Theorem 1. Consider the closed-loop system (31) that is generated using the estimation (24) and the control (27) and consider the parameter estimation error (32). Assume that Assumption 1 is satisfied. Then, for all $\alpha > \frac{\gamma_G}{2} + q\gamma_P$, the following statements hold:

- 1) $(\tilde{x}_{1,k} \dots \tilde{x}_{q,k}) \equiv 0$ is a uniformly Lyapunov stable equilibrium of (31) and (32).
- 2) Let $\tilde{x}_{1,0} \dots \tilde{x}_{q,0} \in \mathbb{R}^4$. Then $x_{i,k}$ and $\theta_{u,i,k}$ are bounded and $\lim_{k \rightarrow \infty} y_k = 0$.

The proof follows along the lines of [18], with necessary adaptations for the modified estimator scheme. A concise proof sketch is given in Appendix A. Note that the proof does not introduce any restrictions for $\tilde{x}_{1,0} \dots \tilde{x}_{q,0}$. Therefore, part 2) of Theorem 1 holds globally, which means that

- 1) y_k converges to zero for all initial parameter estimates $x_{1,0} \dots x_{q,0}$.
- 2) It is always possible to find α such that $\alpha > \frac{\gamma_G}{2} + q\gamma_P$ holds and (32) is fulfilled.

D. Parameter convergence

Convergence of $x_{i,k}$ to the true parameters x_i^* is neither required by the stability proof, nor is it implied by it. However, studying when these parameters converge to their actual true value will be beneficial for the modifications that are proposed in the following sections. Consider the following Proposition.

Proposition 1. ([23]) Consider the harmonic mode i and assume J_k is $\mu_{i,k}$ -strongly convex and $L_{i,k}$ -smooth in x_i . Then, if the learning rate is chosen as

$$\gamma_G, \gamma_P \leq \frac{2}{\mu_{i,k} + L_{i,k}}$$

for all k , then the adaptive law (24) generates a sequence $x_{i,k}$ such that

$$\|x_{i,k} - x_i^*\| \leq \rho_{i,k}^k \|x_{i,0} - x_i^*\|$$

with

$$\rho_{i,k} = 1 - \frac{2 \min(\gamma_G, \gamma_P) \mu_{i,k} L_{i,k}}{\mu_{i,k} + L_{i,k}}.$$

Since J_k is twice differentiable, $\mu_{i,k}$ and $L_{i,k}$ can be determined as minimum and maximum eigenvalue of the Hessian $H_{i,k}$ of J_k . However, note that if J_k is defined as in (22), then

$$H_{i,k} = \frac{\partial^2 J}{\partial x_{i,k}^2} = \eta_k w_{i,k}^\top w_{i,k}, \quad (33)$$

which is rank deficient. Thus, Proposition 1 is not applicable to (22) and no statement about parameter convergence can be made.

To circumvent this issue, dynamic regressor extension can be applied [24], [25]. Note that to uniquely identify four parameters in a regression problem, at least four linearly independent measurement equations are required. When having only one measurement at each k , a widely applied technique is to filter this sequence with four linearly independent linear filters, thus giving four linearly independent sequences which yield a well-posed problem. Consider

$$\mathcal{H}(z) = [1 \ \mathcal{H}_1(z) \ \mathcal{H}_2(z) \ \mathcal{H}_3(z)]. \quad (34)$$

with

$$\mathcal{H}_1(z) = \frac{(1 - T_1)z}{z - T_1}. \quad (35)$$

Distinct values of the time-constants T_1 are chosen to guarantee linear independence among the generated filtered signals. Define

$$\psi_k := \mathcal{H}[y_k] \in \mathbb{R}^4, \quad \Phi_{i,k} := \mathcal{H}[w_{i,k}] \in \mathbb{R}^{4 \times 4} \quad (36)$$

and

$$J_k(x_k) = \frac{\eta_k \|\psi_k - \sum_{i=1}^q \Phi_{i,k}^T x_{i,k}\|^2}{2}. \quad (37)$$

Then,

$$H_{i,k} = \eta_k \Phi_{i,k}^T \Phi_{i,k}, \quad (38)$$

and thus, regularity of the Hessian matrix can be achieved.

Note that $H_{i,k}$ may still become rank deficient, for instance when $w_{i,k} \equiv 0$. Hence, the data must still satisfy some excitation requirements. In contrast, if $H_{i,k}$ has full rank and hence, $\rho_{i,k} < 1$, $w_{i,k}$ must have been sufficiently rich. Therefore, a phase of iterations where $\rho_{i,k} < 1$ indicates a phase of qualitative parameter updates and therefore, a good estimation phase. This intuition will be significant for later proposed modifications of the estimation scheme.

IV. DELTA LEARNING BASED FEEDFORWARD ESTIMATION

In non-adaptive HC, it is well known that the phase of the model used for the control law $\angle G_{u \rightarrow y}(\omega_i)$ and the phase of the true system $\angle G_{u \rightarrow y}(\omega_i)^*$ must lie within a 90° margin to guarantee stability [17]. In contrast, the adaptive scheme ensures stability for all parameter initializations, even when they are arbitrary bad. However, while preserving stability, deviations from the $\pm 90^\circ$ range may still degrade transient performance drastically. This effect is particularly relevant during speed changes, where $\angle G_{u \rightarrow y}(j\omega_i)$ shifts due to its frequency dependence. The stable range shifts accordingly, requiring time for the estimated parameters to adapt. To counteract this effect, this section introduces a delta learning approach that integrates a LUT-based feedforward estimation. An adaptive LUT is proposed that continuously updates during operation and reuses stored parameter values at previously visited operating points.

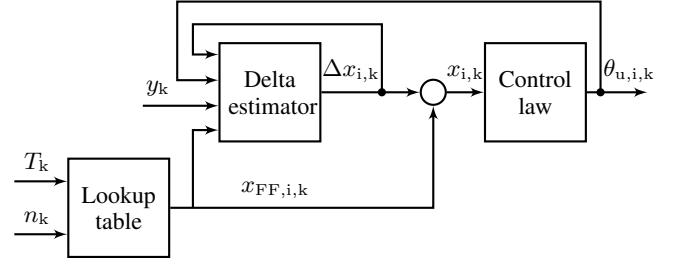


Fig. 4. Delta learning adaptive controller.

A. Integration of delta learning into the harmonic controller

Recall that the adaptive controller consists of an estimator that calculates $x_{i,k+1}$ based on y_k and the previous output of the controller $\theta_{u,i,k}$, along with a control law that computes $\theta_{u,i,k+1}$ based on $x_{i,k+1}$. Figure 4 shows how this adaptive controller is extended to incorporate the delta learning concept. The LUT provides feedforward parameter estimates $x_{FF,i,k}$ based on the current operating point, which is defined by the torque T_k and the rotor speed n_k .

Instead of using (22), we consider the shifted optimization problem

$$\min_{\Delta x_{i,k}} J(\Delta x_{i,k}) = \frac{\eta_k \|y_k - \sum_{i=1}^q w_{i,k}^T (x_{FF,i,k} + \Delta x_{i,k})\|^2}{2} \quad (39)$$

and calculate the gradient w.r.t. $\Delta x_{i,k}$. A key challenge is that infinitely many parameter combinations produce the same control output, so the adaptive controller can achieve correct performance without identifying the true parameter values. This could lead to parameter drift, where the sum $x_{i,k} = x_{FF,i,k} + \Delta x_{i,k}$ diverges from the feedforward estimate, even if the control output remains correct. While the stability proof confirms that this does not lead to instability in the chosen setup, the benefits of improved performance during speed changes – achieved through the delta learning approach – could be compromised. To counteract this, a damping term is introduced into the adaptive law (24), resulting in the modified adaptive law

$$\Delta x_{i,k+1} = (1 - \sigma) \Delta x_{i,k} + \Gamma w_{i,k} \epsilon_k, \quad (40)$$

with the scalar design parameter $\sigma > 0$. Note that this modification is known as σ -modification or leakage and is common to enhance robustness of adaptive control schemes [22], [26].

B. Lookup table setup

Initially, the LUT is populated with identified parameters. Then, it is subsequently updated online.

1) *Transfer function $G_{u \rightarrow y}$* : The first two parameters in (20) correspond to the real and imaginary parts of $G_{u \rightarrow y}(j\omega_i)$, which vary with the speed n , but not with torque T . They are initialized offline by measuring at least two different HSS responses and calculating the parameters via regression.

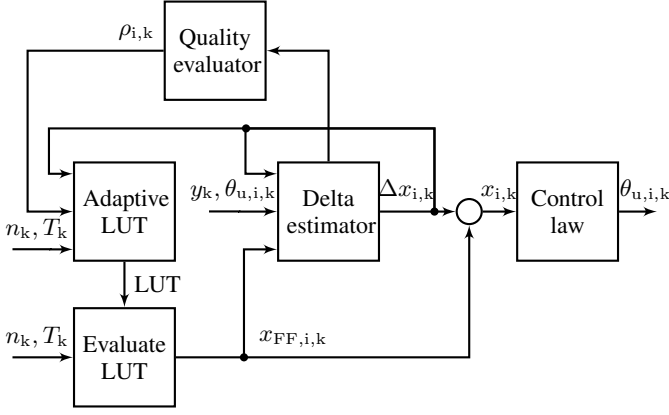


Fig. 5. Adaptive delta learning structure.

2) *Disturbance parameters* $\theta_{p,s}$ and $\theta_{p,c}$: The disturbance parameters depend on both n and torque T and are stored in a two-dimensional LUT. They are initialized similarly from offline measurements at selected support points.

For both cases, feedforward parameter values at operating points between the support points are obtained via linear (for G) or bilinear (for θ_p) interpolation, and extrapolated if outside the grid.

C. Online-adaptation of the lookup table

Note that the scheme with the shifted optimization problem (39) heavily relies on an accurate true parameter prediction. Wrong parameter estimates may even have a detrimental effect on the delta-learning approach. This is especially critical in e-drive systems, where the system behavior is inherently changing during its lifetime due to aging effects. Therefore, we propose an online-adaptation scheme of the LUT.

Crucially, the LUT shall be only updated, when (i) the feedforward parameters deviate from the actual estimated parameters $x_{FF,i,k} + \Delta x_{i,k}$, and (ii), if the data is informative enough. Point (i) is addressed by simply stopping any LUT-updates when $\Delta x_{i,k} = 0$. To achieve point (ii), we leverage the convergence rate $\rho_{i,k}$ which is obtained from Proposition 1. Following the discussions of Subsection III-D, if $\rho_{i,k} < 1$, then the data is suitable for parameter updates and a LUT update is desirable. The smaller $\rho_{i,k}$ the better the regression equations are conditioned and the larger the LUT update shall be.

Consider Figure 5. Compared to the structure shown in Figure 4, two additional blocks are introduced. The estimation quality is evaluated in the "Quality Evaluator" block, which leverages internal properties of the delta estimator to compute $\rho_{i,k}$.

The LUT is now generated by the new "Adaptive LUT" block, which performs the LUT update following

$$\text{LUT}(n_k, T_k) \leftarrow \text{LUT}(n_k, T_k) + (1 - \rho_{i,k}) \beta \Delta x_{i,k}, \quad (41)$$

where β is the learning rate. The LUT is continuously updated as long as $\rho_{i,k} < 1$ and $\|\Delta x_{i,k}\| > 0$. In other words, updates occur when the estimator is reliable and detects a discrepancy between the feedforward parameters and the true parameters.

Remark. We emphasize that dynamic regressor extension is only applied to compute $\rho_{i,k}$ for the dynamic regressor extension and *not* in the control law introduced in Subsection III-B. The main reason is the limited computational budget imposed by the typically short sampling times in e-drive systems. The LUT adaptation is not real-time critical and thus, dynamic regressor extension may be applied here.

D. Active learning

Parameter convergence requires sufficient excitation, i.e. $\rho_{i,k} < 1$. However, since the control law (27) enforces $y = 0$, a lack of excitation will eventually be achieved by design. To address this, an active learning law is introduced. It is well known that for a n -th order system linear in its parameters, $\frac{n}{2}$ distinct frequencies in the reference signal are sufficient [27]. Thus, consider the following excitation law

$$\theta_{u,i,k} = G_{i,k}^{-1} (Y_{\text{des},i,k} - \theta_{p,i,k}), \quad (42)$$

with $Y_{\text{des},i,k}$ being an excitation signal

$$Y_{\text{des},i,k} = \begin{bmatrix} A_{a1,i,k} \cos(\omega_{a1,i,k} k t_s) \\ A_{a2,i,k} \cos(\omega_{a2,i,k} k t_s) \end{bmatrix}, \quad (43)$$

containing two distinct frequencies $\omega_{a1,i,k} \neq \omega_{a2,i,k}$. This enforces

$$y_k = \sum_{i=1}^q f_{i,k}^T Y_{\text{des},i,k}, \quad (44)$$

which ensures sufficient excitation.

Now note that permanent excitation is desirable for parameter convergence on the one hand, but undesirable on the performance level on the other hand, since y still reflects an NVH signal. Thus, active learning is activated only if $\Delta x_{i,k} \neq 0$ and excitation is insufficient. The amplitudes are set as

$$A_{a1,i,k} = A_{a2,i,k} = \max\left(0, \frac{\epsilon - (1 - \rho_{i,k})}{\epsilon}\right) \delta \|\Delta x_{i,k}\|, \quad (45)$$

with tuning factor $\delta > 0$ and threshold $\epsilon > 0$. If $1 - \rho_{i,k} \geq \epsilon$, excitation is sufficient and active learning is disabled.

Thus, the delta learning approach with adaptive LUT ensures that $\Delta x_{i,k} \rightarrow 0$, while active learning is only applied when necessary.

V. SIMULATION RESULTS

This section presents simulation results for the concepts introduced in Section III. The results are obtained from a closed-loop simulation in MATLAB/Simulink, which includes a simulation model of the PSM and an implementation of a Field Oriented Controller (FOC) K to achieve the control loop presented in Figure 1. The unknown NVH transfer behavior is modeled as a second order filter, which takes \dot{i}_q as its input. Additionally, the disturbance p is modeled as a sinusoidal signal in the 12th electrical harmonic frequency. This disturbance is added to the output of the NVH transfer function and yields y . The HC controllers are implemented and connected as described in Section III. To enhance realism, random noise is added to the rotational speed, the PSM currents, and the measured NVH signal y . The amplitudes of the disturbance

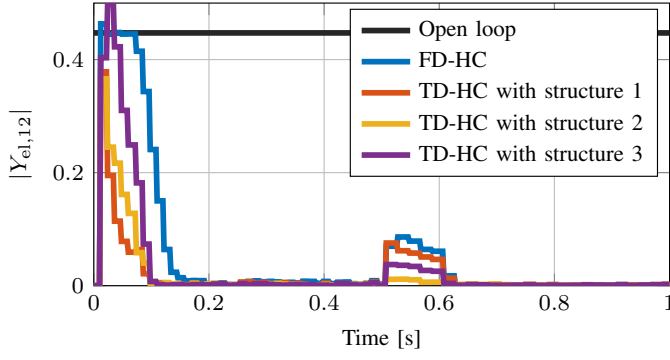


Fig. 6. Reduction of the 12th electrical harmonic in y comparing the time-domain control structures with the benchmark controller.

TABLE II

PERFORMANCE INDICATORS FOR DIFFERENT CONTROL STRUCTURES.

Performance Indicator	FD	TD S1	TD S2	TD S3
Time until $ Y_{el,12} $ is ≤ 0.05	0.132	0.084	0.084	0.096
Mean of $ Y_{el,12} $	0.052	0.019	0.017	0.03
Maximum $ Y_{el,12} $ after 0.5s	0.086	0.076	0.012	0.037
Mean of $ Y_{el,12} $ in Interval 1	0.005	0.003	0.002	0.002
Mean of $ Y_{el,12} $ in Interval 2	0.001	0.001	0.001	0.001

Interval 1: $t = [0.2\text{s}, 0.5\text{s}]$, Interval 2: $t = [0.7\text{s}, 1.0\text{s}]$, FD: frequency-domain, TD: time-domain

and the random noise are chosen to match the levels observed on the testbench, which is introduced in the next section.

In Figure 6, the results are shown for all three control structures, along with the comparison of an adaptive frequency-domain HC controller [16] as benchmark. These results are derived from a simulation where the rotational speed is set to $n_{\text{mech}} = 1000$ rpm for the first 0.5s and then reduced to $n_{\text{mech}} = 800$ rpm for the remaining 0.5s. The presented signals for $|Y_{el,12}|$ – the amplitudes of the 12th electrical harmonic in y – are the result of a DFT analysis performed at the end of each electrical period, which leads to the discrete update steps of the signal. For each control structure, the gain γ is selected through a basic parameter tuning process to ensure that each structure performs well individually. Table II evaluates the results based on five performance indicators related to convergence speed and steady-state error.

Among the three time-domain control structures, no major differences in performance are observed; variations due to different gains or initial conditions are larger than differences between the structures themselves. All three, however, outperform the benchmark controller in terms of faster convergence and lower mean values of $|Y_{el,12}|$.

VI. TESTBENCH RESULTS

In this section, the adaptive time-domain HC, along with its extensions, is examined on the testbench. In all presented results, the rotational speed n_{mech} , the torque T and the measured laser signal y are given normalized by scaling factors.

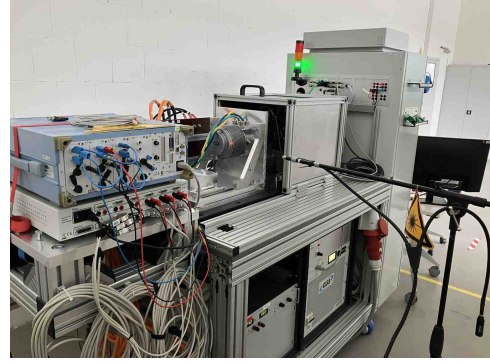


Fig. 7. Testbench setup.

A. Testbench setup

The testbench setup is shown in Figure 7. It shows the Laser Doppler Vibrometer (LDV) measuring NVH emissions in the form of surface vibrations on the housing of the used 48V PSM. The PSM is coupled to a load machine, which regulates the rotational speed to maintain a constant reference value. The controller is implemented in MATLAB/Simulink and online computation is performed on a dSPACE RTI 1007 setup. The sampling rate is set to 10 kHz, corresponding to a sampling time of $t_s = 100\mu\text{s}$. To evaluate NVH reduction under different conditions, various operating points are tested in the experiment to assess the performance of the controllers. This experiment is well-suited for controller evaluation, as all parameters estimated online vary throughout the experiment. Here, mainly the results of reducing the 12th electrical harmonic are presented. In Subsection VI-F, it is demonstrated how the approach can be applied to reduce multiple harmonics.

B. Open loop experiment

To demonstrate the nominal NVH pollution, an open loop experiment without HC is performed. The results of this experiment using the control loop without HC are shown in Figure 8. The third subplot shows the amplitude of the laser signal y in the 12th electrical frequency for three runs of the same experiment. The complete frequency spectrum of y over all three rotational speeds is shown in Figure 9. In all three intervals, the most prominent frequency components are the 2nd and 12th electrical harmonics.

C. Adaptive time-domain harmonic control

Here, the experiment is repeated with the adaptive time-domain HC deployed. Figure 10 shows the outcomes of three runs of the same experiment. Due to space reasons, only the results for structure 1 are displayed, however, we note that the experiment outcomes do only differ slightly. In fact, the discrepancy among different runs for the same control structure – originating from different parameter initializations – is larger than the differences among the structures themselves. Thus, the insights discussed here for Structure 1 also apply to the other two structures. The 12th electrical harmonic is significantly reduced for most of the duration, while the performance after the speed change from 0.6 p.u. to 1 p.u. varies considerably

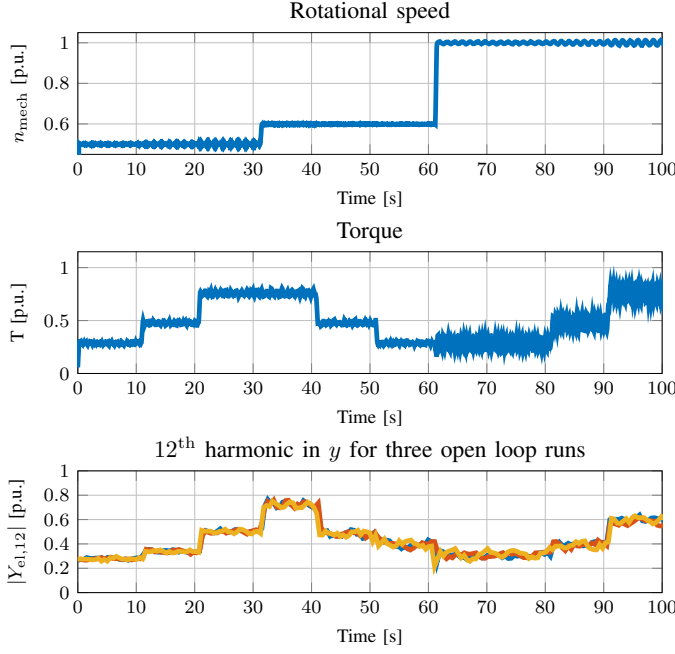


Fig. 8. Open loop experiment: Rotational speed, torque and the amplitude of the 12th electrical harmonic in the laser signal.

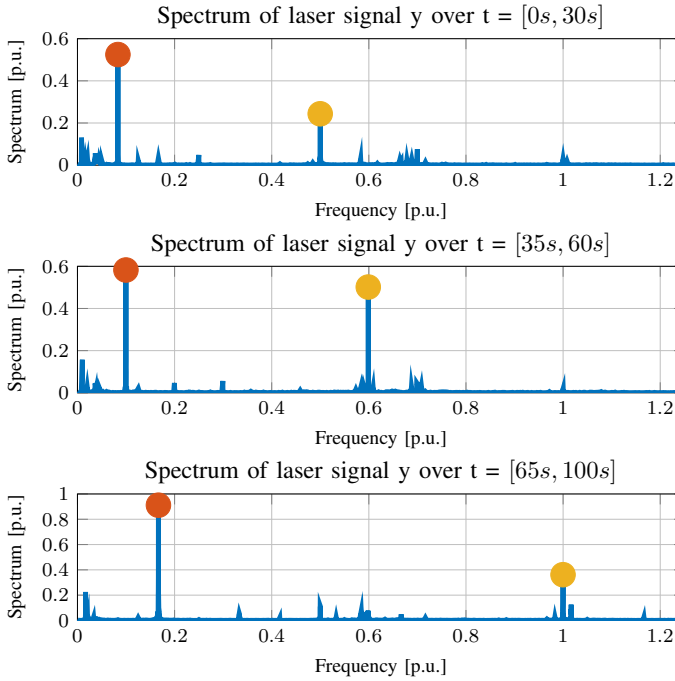


Fig. 9. Frequency spectrum of the laser signal over the different constant speed intervals from an open loop testbench experiment. Blue shows the spectrum; red and yellow markers highlight the 2nd and 12th harmonics, respectively.

between runs. For the different runs, the same controller with the same parameterization is used, with the initial parameter values being the only difference.

To explain the spikes around 60 seconds, and why only run 1 and 2 are affected, observe Figure 11 that shows the identified and estimated phase $\angle \hat{G}_{u \rightarrow y}(j\omega)$. Recall that outside a phase

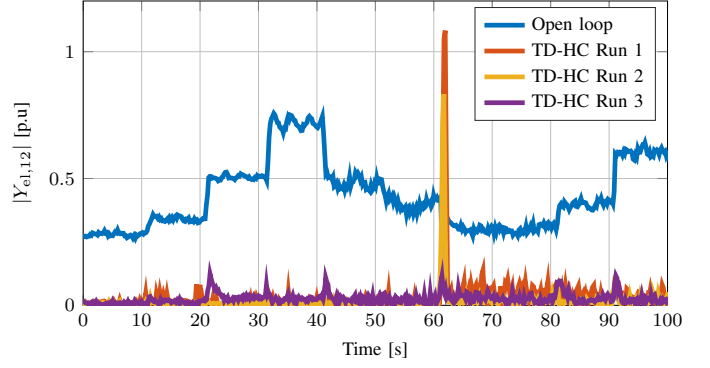


Fig. 10. Reduction of the 12th electrical harmonic in the laser signal.

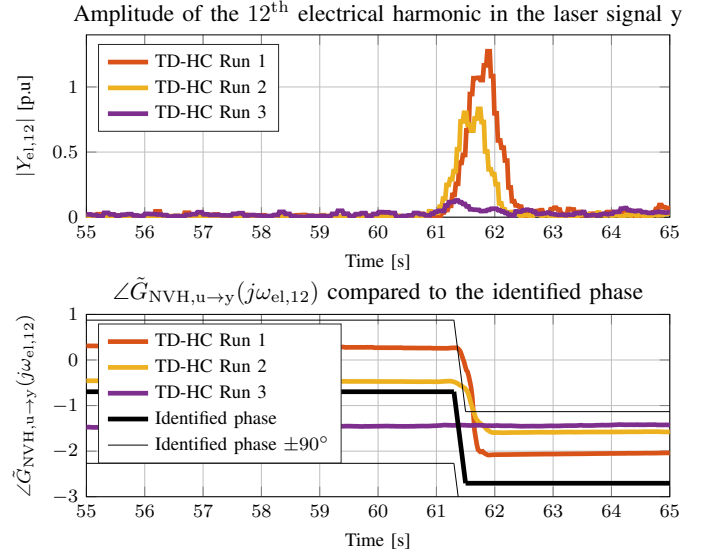


Fig. 11. Amplitude $|Y_{el,12}|$ and the estimated phase of $G_{NVH,u \rightarrow y}(j\omega_{el,12})$ compared to the identified phase during the speed change.

range of $|\angle G_{u \rightarrow y}^*(j\omega) - \angle \hat{G}_{u \rightarrow y}(j\omega)| < 90^\circ$, the nominal HC becomes unstable. We indeed observe that our adaptive formulation can leave this range without harming stability, but with detrimental effects on the transient performance. In contrast, observe how run 3 stays within the nominal stable range and thus, shows only a mild spike in the amplitude.

D. Delta learning approach

Note that the observations in Figure 11 motivate the use of the identified parameters as feedforward estimates in the proposed delta learning scheme described in Section IV. The results of five experimental runs are illustrated in Figure 12. The results indicate a significant reduction in the 12th electrical harmonic across all experiment runs throughout the complete duration of the experiment.

Crucially, observe how the spike from Figure 10 can be successfully mitigated, highlighting the effect of the delta learning approach. This complies with Figure 13, where again the phase difference of identified and estimated system is displayed. Observe in the third subplot how the estimated phase, consisting of prior information plus delta estimation,

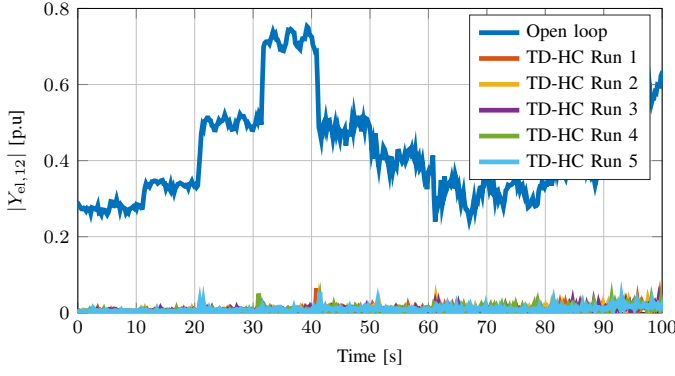


Fig. 12. Reduction of the 12th electrical harmonic in the laser signal using control Structure 1 with the delta learning approach.

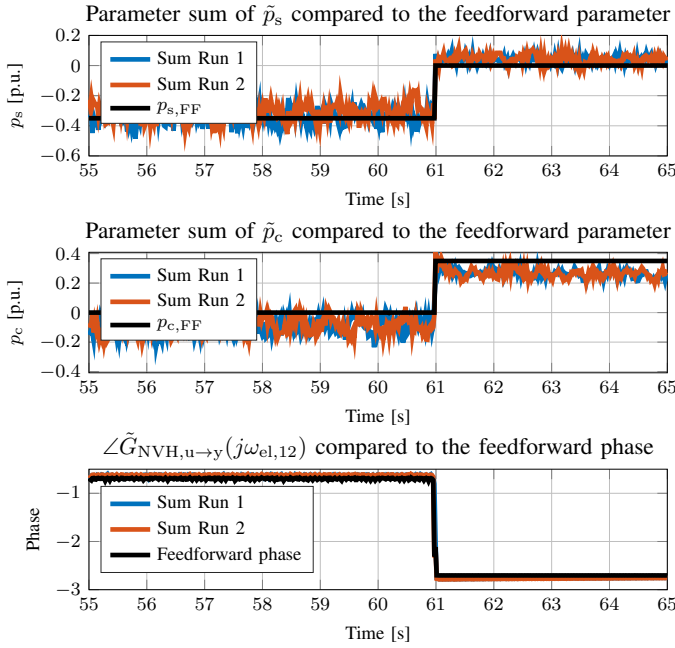


Fig. 13. Parameter sum used in the controller compared to feedforward parameter value using control Structure 1 with the delta learning approach.

now aligns well with the identified phase of the system, in contrast to Figure 11. Moreover, observe in the first two subplots how incorrect feedforward parameters are counteracted by the delta estimate. In particular, the delta estimator captures small high-frequency changes in the parameters.

E. Online-adaptation of the lookup table

Here, testbench results for the online adaptation of the LUT from Subsection IV-C in combination with active learning from Subsection IV-D are presented. In Figure 14, results are shown for a testbench experiment operated at two operating points with different torques, each tested twice. Initially, $\theta_{p,s,FF}$ and $\theta_{p,c,FF}$ show a large deviation from the true parameters $\theta_{p,s}^*$ and $\theta_{p,c}^*$ due to incorrect LUT entries. The results demonstrate that when an operating point with significant deviation is reached, the delta estimator estimates the difference between the feedforward and true parameters.

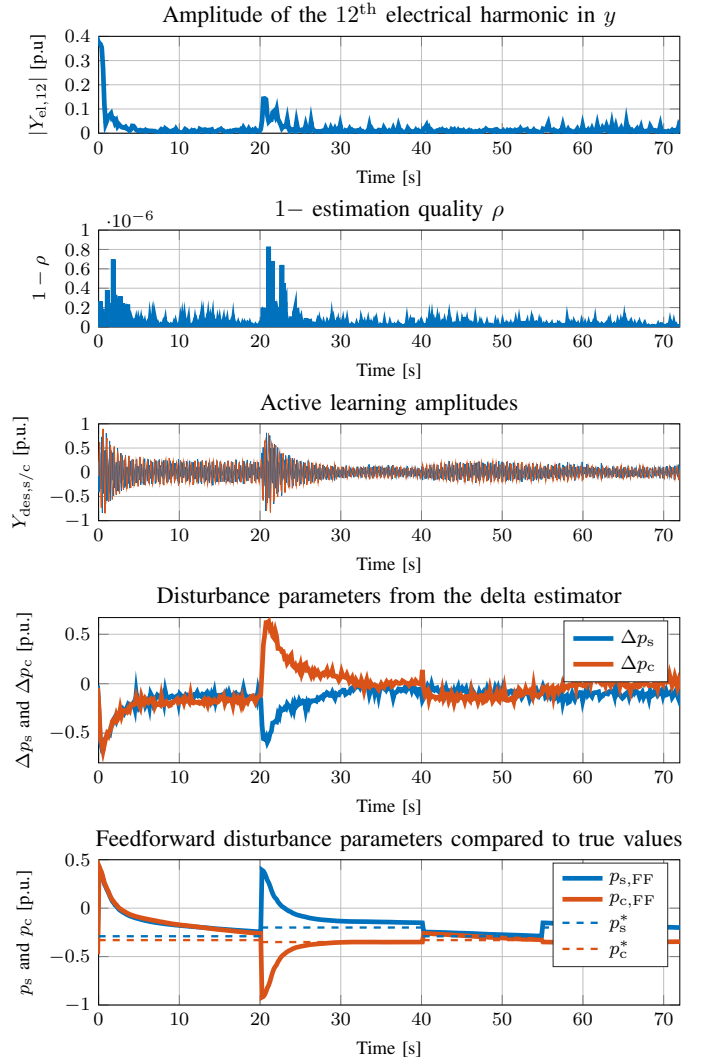


Fig. 14. Reduction of the 12th electrical harmonic in the laser signal using the delta learning approach with online-adaptation of the lookup table.

This is achieved by enabling active learning which leads to a high estimation quality. The LUT is updated, reducing the deviation between the feedforward and true parameters, which in turn lowers the delta parameters. When the operating point is reached a second time, performance in reducing the 12th electrical harmonic improves significantly, as shown by the performance indicators in Table III.

TABLE III
PERFORMANCE INDICATORS FOR REACHING AN OPERATING POINT WITH INCORRECT FEEDFORWARD ESTIMATES AND A SECOND TIME WITH UPDATED VALUES.

Performance Indicator	First time	Second time
Maximum of $ Y_{el,12} $ for $T = 0.5$ p.u.	0.4068	0.0314
Maximum of $ Y_{el,12} $ for $T = 0.3$ p.u.	0.1436	0.0436
Mean value of $ Y_{el,12} $ for $T = 0.5$ p.u.	0.0267	0.0097
Mean value of $ Y_{el,12} $ for $T = 0.3$ p.u.	0.0202	0.0116

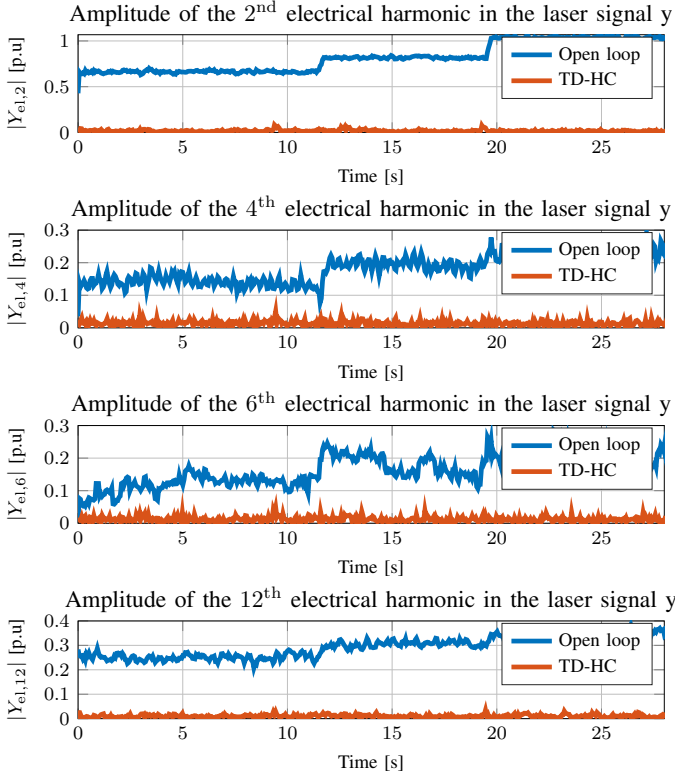


Fig. 15. Simultaneous reduction of multiple electrical harmonics.

F. Reduction of multiple frequencies

Figure 15 illustrates the results for reducing four different disturbance frequencies simultaneously for an experiment where the operating point is changed twice. It is evident that the 2nd, 4th, 6th and 12th electrical harmonics can be successfully reduced in parallel.

VII. CONCLUSION

This work advances adaptive time-domain HC from theory to practice for NVH mitigation in electric drives. Three control structures were developed to integrate the adaptive controller into existing loops, and the estimation scheme was refined to reduce computational effort for embedded use.

Simulations and testbench experiments confirm faster convergence than frequency-domain HC, but also reveal limitations during rapid speed changes. To ensure robustness across operating points, a delta learning scheme was introduced that combines the adaptive controller with a LUT-based feedforward estimator, complemented by an adaptive LUT for lifetime robustness through online updates.

Future work could include a rigorous stability analysis of the extended delta learning structure to ensure that the combination of the adaptive controller and adaptive LUT does not introduce undesired interactions in the overall system. In addition, while the adaptive time-domain HC with delta learning has shown promising performance, other adaptive control concepts recently proposed in the literature – such as sliding mode control [28] or predictive cost adaptive control [29] – could be explored.

APPENDIX A

PROOF SKETCH OF THEOREM 1

Proof. Subtracting αx_i^* from both sides of (24) yields

$$\tilde{x}_{i,k+1} = \tilde{x}_{i,k} + \Gamma w_{i,k} \epsilon_k \quad (46)$$

Considering the individual estimation errors of (32) as

$$\tilde{G}_{i,k} = G_{i,k} - \alpha G_i^* \quad \tilde{\theta}_{p,i,k} = \theta_{p,i,k} - \alpha \theta_{p,i}^*, \quad (47)$$

and splitting (46) yields

$$\tilde{G}_{i,k+1} = \tilde{G}_{i,k} + \gamma_G \eta_k W_{G,i,k} \bar{y}_k \quad (48a)$$

with

$$W_{G,i,k} = \begin{bmatrix} a & -b \\ b & a \end{bmatrix}, \quad \begin{aligned} a &= \theta_{u,s,i,k} s_{i,k} + \theta_{u,c,i,k} c_{i,k} \\ b &= \theta_{u,s,i,k} c_{i,k} - \theta_{u,c,i,k} s_{i,k} \end{aligned} \quad (48b)$$

and

$$\tilde{\theta}_{p,i,k+1} = \tilde{\theta}_{p,i,k} + \gamma_p \eta_k \begin{bmatrix} s_{i,k} \\ c_{i,k} \end{bmatrix} \bar{y}_k \quad (48c)$$

for $s_{i,k} = \sin(\omega_i k t_s)$ and $c_{i,k} = \cos(\omega_i k t_s)$. Defining the Lyapunov function measuring all parameter estimation errors

$$V(\tilde{x}_{1,k} \dots \tilde{x}_{q,k}) = \frac{2}{\gamma_p} \sum_{i=1}^q \|\tilde{\theta}_{p,i,k}\|^2 + \frac{1}{\gamma_G} \sum_{i=1}^q \|\tilde{G}_{i,k}\|_F^2 \quad (49)$$

the corresponding Lyapunov difference is

$$\Delta V(k) = V(\tilde{x}_{1,k+1} \dots \tilde{x}_{q,k+1}) - V(\tilde{x}_{1,k} \dots \tilde{x}_{q,k}). \quad (50)$$

Using straightforward reformulations and noting from (25) that $\eta_k \leq 1$ and $\eta_k \sum_{i=1}^q \|\theta_{u,i,k}\|^2 \leq 1$, one obtains the bound

$$\Delta V(k) \leq -4\eta_k \left(\alpha - q\gamma_p - \frac{\gamma_G}{2} \right) y_k^2. \quad (51)$$

Since this is the same bound as in [18], all claims of Theorem 1 follow by the standard arguments in [18]. \square

REFERENCES

- [1] J.-B. Dupont and V. Lanfranchi, “Noise radiated by a permanent magnet synchronous motor: Simulation methodology and influence of motor defects,” in *International Conference on Electrical Machines*, 2014.
- [2] R. Islam, I. Husain, A. Fardoun, and K. McLaughlin, “Permanent magnet synchronous motor magnet designs with skewing for torque ripple and cogging torque reduction,” in *IEEE Industry Applications Annual Meeting*, 2007.
- [3] D. Schröder, *Elektrische Antriebe - Regelung von Antriebssystemen*. Springer Berlin Heidelberg, 2015.
- [4] A. Langheck and C. Udo, *Reduzierung von Vibrationen und Pendelmomenten in permanenterregten Synchronmaschinen mit harmonischen Strömen*. PhD thesis, 2024.
- [5] S. Bittanti and L. Moiraghi, “Active control of vibrations in helicopters via pole assignment techniques,” *IEEE Transactions on Control Systems Technology*, vol. 2, no. 4, pp. 343–351, 1994.
- [6] D. Patt, L. Liu, J. Chandrasekar, D. S. Bernstein, and P. P. Friedmann, “Higher-harmonic-control algorithm for helicopter vibration reduction revisited,” *Journal of Guidance, Control, and Dynamics*, vol. 28, no. 5, pp. 918–930, 2005.
- [7] L. Lu and H. Zhao, “Active impulsive noise control using maximum correntropy with adaptive kernel size,” *Mechanical Systems and Signal Processing*, vol. 87, pp. 180–191, 2017.
- [8] Y. H. Guan, W. S. S. Jr, T. C. Lim, and M. Li, “Experimental analysis of an active vibration control system for gearboxes,” *Smart Materials and Structures*, vol. 13, p. 1230, sep 2004.
- [9] M. Bodson, A. Sacks, and P. Khosla, “Harmonic generation in adaptive feedforward cancellation schemes,” *IEEE Transactions on Automatic Control*, vol. 39, no. 9, pp. 1939–1944, 1994.

- [10] J. B. Hoagg, M. A. Santillo, and D. S. Bernstein, "Discrete-time adaptive command following and disturbance rejection with unknown exogenous dynamics," *IEEE Transactions on Automatic Control*, vol. 53, no. 4, pp. 912–928, 2008.
- [11] S. Elliott, C. Boucher, and P. Nelson, "The behavior of a multiple channel active control system," *IEEE Transactions on Signal Processing*, vol. 40, no. 5, pp. 1041–1052, 1992.
- [12] J. T. Pearson, R. Goodall, and I. Lyndon, "Active control of helicopter vibration," *Comput. Control Eng. J.*, vol. 5, no. 6, pp. 277–284, 1994.
- [13] P. Friedmann and T. Millott, "Vibration reduction in rotorcraft using active control: A comparison of various approaches," *Journal of Guidance, Control, and Dynamics*, vol. 18, pp. 664–673, 07 1995.
- [14] C. Knospe, R. Hope, S. Tamer, and S. Fedigan, "Robustness of adaptive unbalance control of rotors with magnetic bearings," *Journal of Vibration and Control*, vol. 2, no. 1, pp. 33–52, 1996.
- [15] M. Kamaldar, "Discrete-time adaptive control algorithms for rejection of sinusoidal disturbances," 2018.
- [16] M. Kamaldar and J. B. Hoagg, "Multivariable adaptive harmonic steady-state control for rejection of sinusoidal disturbances acting on an unknown system," in *American Control Conference*, 2016.
- [17] S. Pigg and M. Bodson, "Adaptive algorithms for the rejection of sinusoidal disturbances acting on unknown plants," *IEEE Transactions on Control Systems Technology*, vol. 18, no. 4, pp. 822–836, 2010.
- [18] M. Kamaldar and J. B. Hoagg, "Adaptive harmonic control for rejection of sinusoidal disturbances acting on an unknown system," *IEEE Transactions on Control Systems Technology*, vol. 28, no. 2, pp. 277–290, 2020.
- [19] M. Abu-Ali, F. Berkel, M. Manderla, S. Reimann, R. Kennel, and M. Abdelrahman, "Deep learning-based long-horizon MPC: Robust, high performing, and computationally efficient control for PMSM drives," *IEEE Transactions on Power Electronics*, vol. 37, no. 10, pp. 12486–12501, 2022.
- [20] D. S. Bernstein, *Matrix Mathematics: Theory, Facts, and Formulas*. Princeton University Press, second ed., 2011.
- [21] M. Harries, A. Woerndle, and R. W. De Doncker, "Low vibrations and improved NVH in permanent magnet synchronous machines due to injection of flux-linkage harmonics," *IEEE Journal of Emerging and Selected Topics in Power Electronics*, vol. 10, no. 2, pp. 1649–1657, 2022.
- [22] P. Ioannou and J. Sun, *Robust Adaptive Control*. Dover Books on Electrical Engineering Series, Dover Publications, Incorporated, 2012.
- [23] Y. Nesterov, *Lectures on Convex Optimization*. Springer Cham, 2018.
- [24] B. Yi and R. Ortega, "Conditions for convergence of dynamic regressor extension and mixing parameter estimators using LTI filters," *IEEE Transactions on Automatic Control*, vol. 68, no. 2, pp. 1253–1258, 2023.
- [25] R. Ortega, S. Aranzovskiy, A. A. Pyrkin, A. Astolfi, and A. A. Bobtsov, "New results on parameter estimation via dynamic regressor extension and mixing: Continuous and discrete-time cases," *IEEE Transactions on Automatic Control*, vol. 66, no. 5, pp. 2265–2272, 2021.
- [26] P. Ioannou and P. Kokotovic, "Instability analysis and improvement of robustness of adaptive control," *Automatica*, vol. 20, no. 5, pp. 583–594, 1984.
- [27] S. Boyd and S. Sastry, "On parameter convergence in adaptive control," *Systems & Control Letters*, vol. 3, no. 6, pp. 311–319, 1983.
- [28] K. Lang, L. Shang, P. Xia, and L. Song, "An excellent harmonic feedforward-sliding mode output feedback hybrid algorithm for helicopter active vibration control," *Journal of Vibration and Control*, vol. 29, no. 15–16, pp. 3528–3543, 2023.
- [29] M. Kamaldar, N. Mohseni, S. Islam, and D. S. Bernstein, "A numerical and experimental investigation of predictive cost adaptive control for noise and vibration suppression," *Mechanical Systems and Signal Processing*, vol. 221, p. 111711, 2024.



Klaus Herburger received the B.Sc. and M.Sc. degrees in engineering cybernetics from the University of Stuttgart, Stuttgart, Germany, in 2021 and 2024, respectively. He conducted his master's thesis at Bosch Research, Renningen, Germany, in cooperation with the Institute for Systems Theory and Automatic Control, University of Stuttgart. Since 2022, he has been with Robert Bosch GmbH, Leonberg, as an engineer in the Advanced Driver Assistance Systems domain.



Fabian Jakob received the B.Sc. and M.Sc. degrees in engineering cybernetics from the University of Stuttgart, Stuttgart, Germany, in 2020 and 2022, respectively. From 2021 to 2022, he worked as a research intern in the electric drive department of Bosch Research. He is currently pursuing the Ph.D. degree at the Institute for Systems Theory and Automatic Control, University of Stuttgart, under the supervision of Prof. Dr. Andrea Iannelli. His research interests are the exploration of robust and adaptive control methods for optimization algorithms.



David Gänzle received his Diploma degree in mechanical engineering from the University of Stuttgart, Germany, in 2007. He joined Robert Bosch GmbH in the same year and is currently working at Bosch Research in Renningen, Germany. His work focuses on the modeling, combination of physics-based and data-driven approaches, and control of electrical drives in heating systems and automotive applications. His research interests include adaptive control, such as noise, vibration, and harshness reduction for electric drives.



Maximilian Manderla received the Diploma degree in mechanical engineering and the Dr.-Ing. degree (Ph.D.) in control systems engineering from the Technical University of Darmstadt, Germany, in 2007 and 2011, respectively. He studied mechanical engineering from the Technical University of Darmstadt and the University of California at Berkeley. He was working with Voith Hydro, Heidenheim, Germany, from 2011 to 2015 with focus on hydroelectric power plant dynamics, simulation, and control. In 2015, he joined Bosch, Renningen, Germany, where he is currently active as a Project Manager in the field of control engineering with emphasis on electrical drives in automotive applications. His research interests include model-predictive and learning-based control.



Andrea Iannelli (Member, IEEE) is an Assistant Professor in the Institute for Systems Theory and Automatic Control at the University of Stuttgart. He completed his B.Sc. and M.Sc. degrees in Aerospace Engineering at the University of Pisa and received his PhD from the University of Bristol. He was also a postdoctoral researcher in the Automatic Control Laboratory at ETH Zurich. His main research interests are centered around robust and adaptive control, uncertainty quantification, and sequential decision-making. He serves the community as Associated

Editor for the International Journal of Robust and Nonlinear Control and as IPC member of international conferences in the areas of control, optimization, and learning.